A mutation in vesicular acetylcholine transporter increases tubulin acetylation compromising axonal transport

Cheng-Shan Kuo[#], Meng-Chieh Wang[#], Odvogmed Bayansan, Syed Nooruzuha Barmaver, Prerana Bhan, and Oliver Ingvar Wagner*

National Tsing Hua University, Institute of Molecular and Cellular Biology, Department of Life Science, Hsinchu, 30013, Taiwan (R.O.C.)

[#]Both authors contributed equally to this manuscript

Running title: UNC-17 affects tubulin PTM and transport

***Corresponding author**:

Dr. Oliver I. Wagner

Professor

National Tsing Hua University

Institute of Molecular and Cellular Biology & Department of Life Science

101, Sec. 2, Kuang-Fu Road, Hsinchu 30013, Taiwan (R. O. C.)

Email: owagner@life.nthu.edu.tw

Phone: +886-3-574-2487, Fax: +886-3-571-5934

Keywords: KIF1A, UNC-104, MEC-17, αTAT1, post-translational modification, tubulin, PTM, UNC-17, VAChT, *C. elegans*, BiFC, bimolecular complementation assay

Conflicts of interest: The authors declare no conflict of interest.

ABSTRACT

Kinesin-3 UNC-104(KIF1A) is the major transporter of synaptic vesicles and genetic defects in this motor are linked to Charcot-Marie-Tooth disease and hereditary spastic paraplegia. In a candidate screen for genes causing neurotransmission defects in *C. elegans* and simultaneously affecting post-translational modification of tubulin, we identified allele *unc-17*(*e245*) significantly elevating tubulin acetylation in neurons. UNC-17 encodes for a VAChT (vesicle acetylcholine transporter) and its human ortholog is implicated in Alzheimer's disease. Elevated tubulin acetylation compromises motility of UNC-104 as well its cargo RAB-3. Motility of UNC-104 improves when knocking down alpha-tubulin acetyltransferase MEC-17(ATAT1) in *unc-17*(*e245*) strains. Conversely, motility of UNC-104 is negatively affected when overexpressing MEC-17 in wild type animals. Critically, transport defects are comparable when exposing nematodes to drugs that inhibit ACh neurotransmission. Both UNC-104 and UNC-17 as well as UNC-104 and MEC-17 colocalize in neurons and bimolecular fluorescence complementation assays (BiFC) reveal physical *in situ* interactions between UNC-104/UNC-17, UNC-104/MEC-17 and UNC-17/MEC-17. We propose a model in which reduced expression of UNC-17 frees MEC-17 from the UNC-104/UNC-17 complex. This leads to increased tubulin acetylation, which in turn negatively affects UNC-104 motility.

Graphical abstract

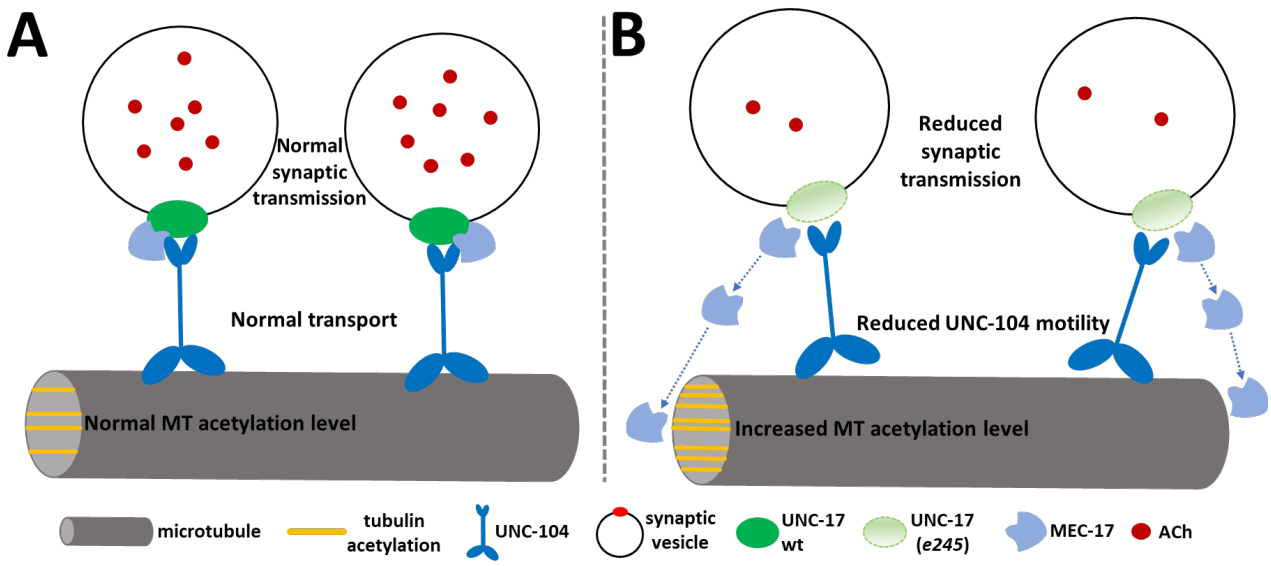

INTRODUCTION

Neurons are highly polarized cells with long projections (termed axon and dendrite) radiating from their cell bodies (also called soma). Since most proteins are synthesized in the soma, a proper intra-cellular transport system must be maintained to ensure that proteins can reach the periphery of neurons for several critical functions such as synaptogenesis, synaptic transmission, axon growth and pathfinding (Guillaud et al., 2020). Axonal transport is a bi-directional transport along microtubule (MT) tracks in which molecular motors of the kinesin class transport cargos to distal regions of neurons (anterograde) or via dyneins back to the soma (retrograde) (Hirokawa et al., 2010). Impaired axonal transport may lead to accumulation of "disease proteins" such as tau, neurofilaments or alpha-synuclein all linked to neurological diseases such as Huntington's disease (HD), Alzheimer's disease (AD) and Parkinson's diseases (PD) (Millecamps and Julien, 2013). Kinesin-3 UNC-104(KIF1A) is the major axonal transporter of RAB-3, synaptotagmin, synaptobrevin and synaptophysin (Hall and Hedgecock, 1991; Maeder et al., 2014), and genetic defects in this motor are linked to KIF1A-associated neurological disorders (KAND) encompassing Charcot-Marie-Tooth (CMT) disease and hereditary spastic paraplegia (HSP) (Chiba et al., 2023; Xu et al., 2018). UNC-104 regulates dendrite branch morphogenesis (Kern et al., 2013; Zhang et al., 2016), density of synapses (Niwa et al., 2016) and is involved in synaptic aging and memory (Li et al., 2016). Homologies between human KIF1A and *C. elegans* UNC-104 are high with 72% positives and 56% identities. UNC-17 encodes for a VAChT (vesicle acetylcholine transporter) that associates with synaptic vesicles (Alfonso et al., 1993) and its human ortholog SLC18A3 (solute carrier family 18 member A3) is linked to AD, HD, pulmonary inflammation and congenital myasthenic syndrome 21 (Banzato et al., 2021; Ferreira-Vieira et al., 2016; Lamond et al., 2021; Smith et al., 2006; Suzuki et al., 2001; Zadrozny et al., 2024). Homologies between human VAChT (SLC18A3) and *C. elegans* UNC-17 are 47% positives and 61% identities. GTP-bound Rab3 acts as an adaptor of UNC-104 to allow transport of various vesicular cargos. At the nerve terminal, Rab3 regulates synaptic vesicle docking and fusion, and facilitates

neurotransmitters release (Binotti et al., 2016). Homologies between human Rab3A and *C. elegans* RAB-3 are impressively high with 81% positives and 73% identities.

Tubulin is the basic component of MTs and their C-terminal ends form unstructured tails emanating from the MTs. Various enzymes can add or remove specific amino acids such as glutamate and tyrosine to and from these tails leading to post-translational modifications (PTMs) of tubulin (Janke and Magiera, 2020). PTMs regulate MT stability and the attachment/detachment rates of MAPs (microtubule-associated proteins) and molecular motors (Genova et al., 2023). Another PTM is acetylation that occurs at lysine-40 of α-tubulin, thus inside the lumen of MTs (Li and Yang, 2015). Acetylation of tubulin weakens the interaction between protofilaments that increases MT flexibility protecting MTs from breakage under stress (Eshun-Wilson et al., 2019). Acetylation of tubulin increases kinesin-1 attachment rates, therefore promoting axonal transport (Godena et al., 2014; Reed et al., 2006). However, the relationship between tubulin acetylation and kinesin-1 motility is still debated, with some studies showing no direct effect of acetylation on kinesin-1 velocity or run length (Kaul et al., 2014; Walter et al., 2012). Acetylation of tubulin is catalyzed by α-tubulin acetyltransferase (ATAT1) (Janke and Magiera, 2020) which is MEC-17 in *C. elegans* (49% positives/64% identities). A mutation in MEC-17 in *C. elegans* leads to variable numbers of protofilaments in touch receptor neurons (Cueva et al., 2012). Besides, MEC-17 regulates the development of synaptic branches by its non-enzymatic domain, and in *mec-17* mutants, synaptic vesicles are decreased at synapses (Teoh et al., 2022). Notably, reduced levels of tubulin acetylation are found in PD, HD and CMT and all of these diseases are linked to disturbed axonal transport. Particularly, decreased tubulin acetylation levels are detected in HD models and patient samples. However, the relationship between tubulin acetylation and axonal transport defects in HD is complex, such as restoring acetylation levels alone does not fully rescue transport impairments (d'Ydewalle et al., 2011; Dompierre et al., 2007; Godena et al., 2014). While some studies reveal decreased tubulin acetylation levels in PD models and patient samples, others have found no significant changes or even increased acetylation levels (Mazzetti et al., 2024).

The direct relation between synaptic transmission and axonal transport is evident from various studies. For example, in *C. elegans*, kinesin-1 UNC-116(KIF5) regulates the delivery and removal of AMPA receptor GLR-1 at postsynapses. Mutated UNC-116 causes changes in surface expression of GLR-1 directly modulating electrophysiological signals (Fan and Lai, 2022; Hoerndli et al., 2013). Conversely, a relation between PTM and axonal transport (and in turn synaptic transmission) has been described, such as that the reduction of tubulin polyglutamylation alters neuronal distribution of KIF1A which in turn directly modulates synaptic transmission (Ikegami et al., 2007). Likewise, activation of AMPAR leads to increased levels of polyglutamylation directly affecting KIF5-based transport (Maas et al., 2009).

In this study, we carried out a candidate screen of various *C. elegans* strains known to display synaptic transmission defects and monitored changes in tubulin PTM in these mutants. We then investigated changes in axonal transport and dissected the underlying molecular mechanisms that link synaptic transmission to tubulin PTM and transport.

RESULTS

Tubulin PTMs are crucial for regulating microtubule dynamics playing a vital role in neuronal health and synaptic function. In a candidate screen for *C. elegans* mutant strains that exhibit synaptic transmission defects causing changes in tubulin PTM, we employed wild type N2 worms as well as 7 different mutant strains: *dat-1* with defects in dopamine neurotransmission (Nass et al., 2002), *eat-4* with defects in glutamate neurotransmission (Avery, 1993), *unc-17* with defects in ACh neurotransmission (Sandoval et al., 2006), *unc-25* with defects in GABA neurotransmission (McIntire et al., 1993), *tbh-1* with defects in octopamine neurotransmission (Alkema et al., 2005), *tdc-1* with defects in tyramine neurotransmission (Alkema et al., 2005), and *tph-1* with defects in serotonin neurotransmission (Sze et al., 2000). Western blots from whole worm lysates revealed a 1.54-fold upregulation in tubulin acetylation in the *unc-17* strain whereas changes in other strains remained insignificant (Fig. 1A+B, Suppl. Fig. S3A). Interestingly, tubulin tyrosination did not change in all strains (Fig. 1A, Suppl. Figs. S1+S3B). We did not screen for changes in glutamylation since in *C. elegans* this

type of PTM is mostly seen in cilia or male sensory neurons (O'Hagan et al., 2022). Employing whole mount immunostaining we further demonstrate that acetylation is 3-fold increased in ALM neurons of *unc-17*(*e245*) mutants (Fig. 1C-E). The gene unc-17 encodes for a synaptic vesicular acetylcholine transporter (VAChT) and the hypomorphic allele *e245* carries a G/C substitution in the 3rd (and last) exon of unc-17 causing the worms to coil-up at all developmental stages with impeded locomotion associated to neurotransmission defects (Alfonso et al., 1993; Sandoval et al., 2006; Zhu et al., 2001). Immunostaining of *unc-17*(*e245*) worms with a monoclonal anti-UNC-17 antibody shows reduced expression of UNC-17 in neurons (Mathews et al., 2021; Sandoval et al., 2006).

To understand the potential impact of altered tubulin PTM on axonal transport, we analyzed motility of the major axonal transporter UNC-104 and its cargo RAB-3 in neurons of living *C. elegans* animals. Particularly, we use the ALM neuron for our observation which has a particularly long axon (up to 0.5 mm) and can be easily identified among other neurons in nematodes (Fig. 1C). Note that in previous studies, we have shown that the characteristics of UNC-104 motility is comparable among various other neurons such as PLM neuron and neurons from the sublateral system (Tien et al., 2011; Wagner et al., 2009; Wu et al., 2016). Intriguingly, motility of both motor (*e1265*;*Punc-104::unc-104::mrfp*) and cargo (N2;*Punc-104::mCherry::RAB-3*) was largely compromised (Fig. 2). Both anterograde and retrograde velocities were reduced (Fig. 2A) reflected by an increase in pausing (Fig. 2B). Also, single run length events (Fig. 2C) as well as total run length (Fig. 2D) was negatively affected by the *unc-17* mutation in both directions (see also Fig. 2E). Since UNC-104 is an anterograde motor, the reduction in retrograde directions is likely based on dynein motility. The "paradox of co-dependence model" explains well this finding: motors are mutually activated by mechanically pulling on each other in opposing directions. If this mechanical activation is lost or reduced, motor activation is diminished (Hancock, 2014).

In previous studies, we identified that UNC-104 tends to form dynamic aggregates along neurons which are likely stations for motor/cargo exchange (Tien et al., 2011; Wagner et al., 2009). We found that in *unc-17*(*e245*) these aggregates are significantly reduced and appear more diffuse (Fig.

3B, E+F). Also, both motor and cargo travel significantly shorter distances in neurons (Fig. 3A+D), an effect that can be visibly seen in neurons (Fig. 3B+C). We then attempted to reduce acetylation in *unc-17*(*e245*) worms by knocking down MEC-17, the acetylase responsible for tubulin acetylation in *C. elegans* neurons (Cueva et al., 2012). As expected, mec-17 knockdown (KD) largely reversed the negative effects on UNC-104 motility in *unc-17* mutants: velocity significantly increased in both directions (Fig. 4A+B), pausing significantly decreased (Fig. 4C) and anterograde total run length significantly increased (Fig. 4D). Conversely, overexpressing MEC-17 in wild type animals led to comparable effects as measured in *unc-17* mutants (Fig. 4, wt;MEC-17 *OEX*). Western blots confirm the reduction of tubulin acetylation in the *unc-17*(*e245*);*mec-17 KD* strain and the increase in tubulin acetylation in the wt;MEC-17 *OEX* strain (Fig. 4G+H, Suppl. Fig. S3C). Note that we were unable to rescue *e245* effects by overexpressing deacetylase HDA-6 (data not shown) which is a homolog of human deacetylase HDAC6 (human histone deacetylase 6) known to reverse the action of ATAT1 (Janke and Magiera, 2020). Nevertheless, we also inhibited ACh transmission in wild type animals using the drug levamisole (an AChR agonist) revealing comparable effects on motor motility as determined for the *unc-17* mutation alone (Fig. 4, wt;Levamisole 1mM). With these data, we are first to disclose the direct negative effect of tubulin acetylation on UNC-104(KIF1A)-mediated axonal transport.

We then inspected expression patterns and colocalization of UNC-104, UNC-17 and MEC-17 (all under their own promoters) in *C. elegans* neurons. From confocal images it is evident that UNC-104 and UNC-17 as well as UNC-104 and MEC-17 colocalize in a large set of head and body neurons including the ALM neuron (Fig. 5). Though colocalization is a critical method to visibly discern the expression of two proteins in animal tissues, we also employed bimolecular fluorescence assay (BiFC) to investigate possible *in situ* interactions of these proteins. In BifC assays, the YFP protein Venus is split into two halves (N-terminal Venus, VN, and C-terminal Venus, VC) and the two test-proteins are fused to each half (Fig. 6H). Complementation of Venus, leading to yellow fluorescent signals, occurs only if these two test-proteins are at least 7-10 nm close to each other,

therefore likely physically interacting (Hsu et al., 2011; Hu and Kerppola, 2003). From Figure 6 it is obvious that distinct Venus signals appear for the BiFC pairs UNC-104/UNC-17, UNC-104/MEC-17 and UNC-17/MEC-17. Also here, we specifically display the ALM neuron that served as a model neuron for transport assays. Based on these results, we develop the following model: MEC-17 forms a transport complex with UNC-17 (Fig. 7A) and in worms carrying the hypomorphic allele *unc-17*(*e245*), MEC-17 will be freed from the complex causing increased tubulin acetylation that negatively affects UNC-104 motility. In addition, since kinesin-3 is known to be activated by cargo binding (Akhmanova and Hammer, 2010; Hummel and Hoogenraad, 2021), improper binding of UNC-17 cargo might disrupt the activation of UNC-104 (Fig. 7B).

DISCUSSION

Axonal transport defects have long been linked to various neurodegenerative diseases including HD, AD and PD (Guillaud et al., 2020; Guo et al., 2020; Surana et al., 2020), and the multiple neurological diseases linked to genetic defects in KIF1A/UNC-104 are classified as KAND (KIF1A-associated neurological disorders) encompassing CMT, ALS and HSP (Ali and Yang, 2020; Brady and Morfini, 2017; Millecamps and Julien, 2013). Vice versa, dysfunction or alteration of neurotransmitter release are linked to neuropathological diseases such as AD and PD (Factor et al., 2017; Francis, 2005; Garcia-Alloza et al., 2005). On the other hand, various studies have shown that synaptic transmission defects alter tubulin PTM (Maas et al., 2009) and, conversely, that tubulin PTM regulates axonal transport (Dunn et al., 2008; Peris et al., 2009; Reed et al., 2006; Wloga et al., 2017). The direct link of UNC-104 to synaptic transmission can be seen in a single point mutation (allele *e1265*) in the motor's C-terminal PH domain (linking the motor to the cargo), causing significant vesicle retention phenotypes that result in a paralyzed and highly uncoordinated nematode (Hall and Hedgecock, 1991; Yonekawa et al., 1998). A homozygous *kif1a* knockout in mouse affects the function of sensory neurons so severely that the animal dies at the embryonic stage (Yonekawa et al., 1998). Similarly, the single amino acid substitution encoded in the hypomorphic allele *unc-17*(*e245*) results in acute neuromuscular function failure leading to paralyzed and coiled-up animals at all developmental stages.

In addition, body size is small, pharyngeal pumping is abnormal and locomotion is uncoordinated (de Castro et al., 2009; Sandoval et al., 2006; Zhu et al., 2001). Interestingly, the human ortholog of the unc-17 gene SLC18A3 (solute carrier family 18 member A3) is implicated in AD, HD, pulmonary inflammation and congenital myasthenic syndrome 21 (Banzato et al., 2021; Ferreira-Vieira et al., 2016; Lamond et al., 2021; Smith et al., 2006; Suzuki et al., 2001; Zadrozny et al., 2024). Besides RAB-3 (Fig. 2+3), SNB-1 (synaptobrevin-1) is a well-described cargo for UNC-104 (Bhan et al., 2020; Tien et al., 2011; Wu et al., 2016) and a genetic interaction between UNC-17 and SNB-1 has been reported by others, suggesting that UNC-17 functions together with SNB-1 to maintain proper packaging and loading of ACh (Sandoval et al., 2006). The effects of ACh agonists such as levamisole (Fig. 4) have been reported by others as well revealing a tight relation between levamisole and RAB-3 motility (Mondal et al., 2011).

The effects of MT acetylation on kinesin-1 motility have been described in various studies. *In vitro* motility assays demonstrate that loss of acetylation on α-tubulin K-40 results in reduced kinesin-1 velocity. In the same study, inhibiting HDAC6 in primary hippocampal cells led to increased tubulin acetylation levels and concomitantly steering the kinesin-1 cargo JIP1 to the neurite tips (Reed et al., 2006). In cultured neurons and *Drosophila* models with pathogenic mutations of LRRK2 Roc-COR, mitochondrial transport was inhibited in both directions with alongside decreased tubulin acetylation. Increasing tubulin acetylation levels through RNAi knockdown of *HDAC6* and *Sirt2* in mutant *Drosophila* restored the axonal transport of mitochondria and locomotion ability (Godena et al., 2014). Besides these studies revealing a positive relation between kinesin-1 motility and tubulin acetylation, one study demonstrated reduced (dynein-mediated) aggresome transport in A549 cell lines after *HDAC6* knockdown (leading to increased acetylation levels). Interestingly, interactions between HDAC6 and dynein has been validated (Kawaguchi et al., 2003). Thus, it is not unlikely that PTM enzymes and motors directly interact as revealed for UNC-104 and MEC-17 in the present study (Figure 6D+E). Due to the ongoing discussion whether α-tubulin K40 acetylation directly enhances the velocity of kinesin-1 and its affinity to MTs, one group compared kinsin-1 motor motility on MTs

reconstituted from acetylated and deacetylated tubulin. As a result, this group has clearly demonstrated that tubulin acetylation alone does not affect kinesin-1 velocity and run length, and that it is rather a combination of various PTMs as well as MAP binding (Walter et al., 2012).

In one study, inhibition of HDAC6 (leading to increased acetylation) in primary human macrophages reduced the anterograde velocity and run length of kinesin-3 KIF1C (Bhuwania et al., 2014) underscoring indeed the tendency of motors from the kinesin-3 class to be negatively affected by acetylation (Fig. 4). Furthermore, our findings of functional interactions between a molecular motor (UNC-104), regulator of neurotransmission (UNC-17), and a PTM enzyme (MEC-17) is supported by reports from other groups. For instance, inhibiting glycine receptor activity in primary hippocampal neurons disturbed the transport of gephyrin (that anchors glycine receptors) to the periphery of neurites. Critically, inhibition of glycine receptors significantly increased tubulin polyglutamylation levels, and depletion of polyglutamylase activity with antibodies prevented the inhibition of gephyrin transport (Maas et al., 2009). This study effectively reveals the relation between synaptic transmission, tubulin PTM and axonal transport. In a greater relation to our study, both overexpression of MEC-17 and mutations in the mec-17 gene led to a significant reduction of synaptic vesicles at synapses in *C. elegans* neurons (Teoh et al., 2022). And in another study, higher MT acetylation levels correlated with the sensitivity to aldicarb (a cholinesterase inhibitor) concomitantly increasing velocities of dense core vesicles in *C. elegans* neurons (Solinger et al., 2010). Moreover, it has been demonstrated that MEC-17 co-distributes with synaptic vesicle precursors in super-resolution images and that MEC-17 localizes to the external surface of vesicles (Even et al., 2019). Critically, it was verified that KIF1A reveals only low affinity to MTs near presynaptic sites. The reason is the enrichment of MT plus-end TIPs (e.g., EB proteins) that increase detachment rates of KIF1A to facilitate proper delivery of precursors to synaptic sites (Guedes-Dias et al., 2019). Therefore, we propose that increased MT acetylation levels in *unc-17* mutants promotes the detachment of UNC-104 at synaptic regions for a more precise delivery of synaptic vesicles to compensate for the decrease of ACh transmitter at synapses (Fig. 7).

MATERIALS & METHODS

C. elegans maintenance, plasmids constructs and generation of strains

Nematodes were maintained at 20°C on NGM agar plates seeded with OP50 *E. coli* according to standard methods (Brenner, 1974). Note that for one experiment (Fig. 4, wt;Levemisole 1mM) we added 10 mM levamisole (#Sigma T1512) to the petri dishes before pouring the (hand warm) NGM agar into them (reaching a final concentration of 1 mM levamisole). If not otherwise mentioned, strains were obtained from the *Caenorhabditis* Genetic Center (Minnesota, USA). *Punc-104::mcherry::rab-3* was designed by amplifying the rab-3 gene from a cDNA library using primers ATGGCGGCTGGCGGACAA (forward) and TTAGCAATTGCATTGCTGTT (reverse). The resulting plasmid was microinjected (using a standard protocol (Mello et al., 1991)) at 50 ng/µl into either N2 or CB933 *unc-17*(*e245*) strains to generate OIW 118 *N2*;*nthEx118*[*Punc-104*::*mCherry*::*rab-3*] and OIW 119 *unc-17*(*e245*);*nthEx119*[*Punc-104*::*mCherry*::*rab-3*], respectively. The existing plasmid *Punc-104::unc-104::mrfp* (Tien et al., 2011) was injected into *unc-17*(*e245*) strain at 80 ng/µl to generate OIW 120 *unc-17*(*e245*);*nthEx120*[*Punc-104*::*unc-104::mrfp*]. OIW 121 *unc-17(e245);nthEx121[Punc-104::unc-104::mrfp]* was generated by crossing *unc-17(e245)* with existing strain *unc-104(e1265);nthEx[Punc-104::unc-104::mrfp]* (Tien et al., 2011) and the strong coiler phenotype of *unc-17*(*e245*) was used for screening after backcrossing. Note that for optimal operation of the Punc104 promoter (thus optimal UNC-104 expression) rather high injection dosages are needed (Tien et al., 2011; Wagner et al., 2009). Indeed, only unc-104 (full-length) plasmid concentrations above 70 ng/µl fully rescues the highly uncoordinated *unc-104*(*e1265*) phenotype (Klopfenstein and Vale, 2004) and neither ectopic expression nor any effects on worm behavior are detected. To generate the transcriptional fusion plasmid *Punc-17::gfp*, the 1.9 kb promoter region of *unc-17* was cloned into the existing pPD95.77 GFP vector plasmid taken from the Andrew Fire Library (a kind gift from Dr. Wu Yi-Chun at NTU) using the aaaaaGCATGCAATGACTAGACGCTGAAG (forward) and aaaaaCTGCAGGAAAATTAAATATTTTAGTGTAAAACTTTTGGG (reverse) primers. To generate the translational fusion plasmid *Punc-17::unc-17::gfp*, the cDNA of *unc-17* was cloned into the

transcriptional fusion plasmid *Punc-17::gfp* using aaaaaaTCTAGAATGGGCTTCAAC-GTGCCCGTC (forward) and aaaaaaGGTACCCTACCACTGCGGATTCAGTGG (reverse) primers. OIW122 *N2;nthEx122[Punc-17::unc-17::gfp;unc-104::unc-104::mrfp]* was generated by microinjecting the *Punc-17::unc-17::gfp* plasmid (80 ng/µl) and *Punc-104::unc-104::mrfp* plasmid (80 ng/µl) into wild type N2 worms for colocalization analysis. The translational fusion plasmid *Pmec-17::mec-17::gfp* was generated by cloning the promoter region of *mec-17* into the existing pPD95.77 GFP vector plasmid using primer aaaaGCATGCgataagaattggtagagcaaagacggc (forward) and aaaaGTCGACgatcgaatcgtctcacaactgatcca (reverse) primers. The genomic DNA of *mec-17* was then cloned into the plasmid using aaaaaCCCGGGatgcaagtcgacgccgacc (forward) and aaaaaTGGCCAac-cacaatggcttgctcgac (reverse) primers. To observe MEC-17 overexpression effects, OIW 123 *N2;nthEx123[Pmec-17::mec-17::gfp;Punc-104::unc-104::mrfp]* was generated by microinjecting the *Pmec-17::mec-17::gfp* plasmid (100 ng/µl) and *Punc-104::unc-104::mrfp* plasmid (90 ng/µl) into N2 wild type worms. For BiFC assays, *Punc-17::unc-17::VC155* and *Punc-17::unc-17::VN173* were generated by subcloning the promoter and cDNA of *unc-17* from aforementioned *Punc-17::unc-17::gfp* into the existing plasmids *Punc-104::VC155* and *Punc-104::VN173* (Hsu et al., 2011), respectively. *Pmec-17::mec-17::VC155* was generated by subcloning the promoter and genomic DNA of *mec-17* from *Pmec-17::mec-17::gfp* into the existing plasmid *Punc-104::VC155*. OIW 124 *N2;nthEx124[Punc-104::unc-104::VN173;Punc-17::unc-17::VC155]* was then generated by microinjecting existing plasmid *Punc-104::unc-104::VN173* (60 ng/µl) (Wu et al., 2016) and above mentioned *Punc-17::unc-17::VC155* (60 ng/µl) plasmids along with roller co-injection marker pRF4(rol-6(su1006)) (50 ng/µl) into N2 worms. OIW 125 *N2;nthEx125[Punc-104::unc-104::VN173;Pmec-17::mec-17::VC155]* was generated by microinjecting *Punc-104::unc-104::VN173* (60 ng/µl) and plasmid *Pmec-17::mec-17::VC155* (60 ng/µl) plasmids along with roller co-injection marker pRF4(rol-6(su1006)) (50 ng/µl) into N2 worms. OIW 126 *N2;nthEx126[Punc-17::unc-17::VN173;Pmec-17::mec-17::VC155]* was generated by microinjecting plasmid *Punc-17::unc-17::VN173* (60 ng/µl) and *Pmec-17::mec-17::VC155* (60 ng/µl) plasmids along with roller

co-injection marker pRF4(rol-6(su1006)) (50 ng/µl) into N2 worms. For a negative control, we injected the *Punc-104::VC155* empty vector plasmid (40 ng/µl) and *Punc-17::unc-17::VN173* plasmid (60 ng/µl) along with roller co-injection marker pRF4(rol-6(su1006)) (50 ng/µl) into N2 worms to generate OIW 127 *N2;nthEx127[Punc-104::VC155EV; Punc-17::unc-17::VN173]*.

RNAi feeding assay

For RNA interference experiments, we employed the RNAi feeding method (Kamath et al., 2001) in which worms are fed by bacteria producing the desired dsRNA. Feeding clones were obtained from the Julie Ahringer's *C. elegans* RNAi feeding library (Source BioScience LifeSciences, USA; a kind gift from the *C. elegans* Core Facility, Taiwan) and sequenced them to determine their correctness. NGM plates containing ampicillin (100 µg/ml) and 1 mM IPTG were inoculated with the respective HT115 *E. coli* strain carrying the appropriate gene insert (flanked by T7 promoters) and grown overnight. 15-20 worms were transferred to the respective RNAi feeding plate and incubated at 20˚C. Worms were then transferred to new RNAi feeding plates every 24 hours and the F1 progeny was used for analysis after day 5. Note that knocking down proteins in neuronal *C. elegans* tissues without the use of "enhancer strains" (such as *rrf-3* or *eri-1*) has been successfully implemented in various studies from this lab (Barmaver et al., 2022; Bhan et al., 2020; Chen et al., 2019; Muniesh et al., 2020; Wu et al., 2016).

Western blot analysis

To perform Western blotting from whole worm lysates, we employed a published protocol (Mahmood and Yang, 2012). Here, 100 µg sample protein is used and membrane blocking is done using milk powder for 2 hours at room temperature (RT). Due to high homology between mouse and *C. elegans* α-tubulin, we use primary anti-acetylated tubulin antibody from mouse (monoclonal 6-11 B-1, T7451 Sigma, 1/1000 dilution) as well as primary anti-tyrosinated tubulin antibody from mouse (monoclonal TUB-1A2, T9028 Sigma, 1/5000 dilution) along with mouse anti-GAPDH antibody (monoclonal 60004-1-Ig, Proteintech, 1/5000 dilution) at 4°C overnight. The secondary anti-mouse antibody

(GTX213111-01, GeneTex) was used at 1/2000 dilution for acetylation, 1/5000 dilution for tyrosination, and 1/5000 dilution for GAPDH detection and incubated at RT for 2 hours. ECL (CyECL Western Blotting Substrate H) was applied for chemiluminescent detection and the membrane was incubated in ECL solution. We used a LAS-4000 Luminescent image analyzer to develop the blots.

Whole mount immunostaining

For whole mount immunostaining, we followed a published protocol (Duerr, 2006). Nematodes are treated with 4% paraformaldehyde in a 2 ml tube and then incubated at 37°C in beta-mercaptoethanol solution for 2 hours. Collagenase is then added to the solution and worms are incubated for an additional 6.5 hours at 37°C. For antibody staining, worms are blocked first for 1 hour at RT using blocking buffer (5% lyophilized serum albumin solution and antibody buffer) and after applying primary antibodies (anti-acetylated 6-11 B-1 1:200) incubated at 4°C overnight. Secondary antibodies (anti-mouse IgG CF488, Sigma) are then used for 2-4 hours at RT and the solution is covered by aluminum foil to protect the worms from light avoiding photobleaching. 10 µl of the sample is then mixed with 10 µl of mounting medium (200 mg n-propyl gallate, 0.3 ml 1 M Tris pH9, 7 ml glycerol, and 2.7 ml ddH_2O) on poly-L-lysine coated glass slide (Sigma) covered with a 22 mm x 22 mm cover slide. A Zeiss LSM780 confocal microscope was employed for imaging worms and ImageJ to determine "corrected total cell fluorescence" with CTCF = Integrated density of selection region – (Area of selection region x Mean fluorescence of background).

Worm imaging and motility analysis

For microscopic observations, worms were immobilized on 2% agarose-coated cover slides, and no anesthetics (such as levamisole) were used. A Zeiss LSM780 confocal laser scanning microscope was employed for imaging worms as shown in Figures 5 and 6. For motility analysis (Figs. 2 + 4), we employed an Olympus IX81 microscope with a DSU Nipkow spinning disk unit connected to an Andor iXon DV897 EMCCD camera for high-speed and long-duration time-lapse imaging (4-5 frames per second). To convert recorded time-lapse sequences into kymographs, we use imaging analysis software NIH ImageJ. The 'straighten plugin' is employed to straighten curved axons, and

after drawing a line over the axon, the plugin 'reslice stack function' is executed to generate kymographs. In kymographs, static particles appear as vertical lines, whereas the slope of a moving particle corresponds to the velocity (speed) of the particle (Fig. 2E). A pause is defined if motors move less than 0.07 μm/s, and each calculated velocity event does not contain any pauses. A moving event is defined as a single motility occurrence typically right after a pause or a reversal, and such an event ends when the motor again pauses or reverses. Note that data shown in Fig. 2 and Fig. 4 were acquired independently by two students (with experiments spaced apart by five years), thus the effect of *unc-17*(*e245*) on UNC-104 motility was well reproduced. Motor cluster analysis (Fig. 3) was carried out using ImageJ's 'area' tool and the 'particle analyze' plugin. To measure travel distances (Fig. 3) of particles in (straightened) neurons, we used ImageJ's 'line tool' to draw a line from the proximal axon hillock to the identified distal particle (Fig. 5A). Intensity correlation quotient (ICQ) (Fig. 5E) was determined by selecting the region of interest using the 'polygonal selection tool' in ImageJ. After background fluorescent intensity subtraction ('subtract background' function), the plugin 'intensity correlation analysis' was used to generate ICQ values. ICQ values range from -0.5 to 0.5 with values close to 0.5 indicating interdependent expression of two fluorophores, values close to 0 implying random expression and values close to -0.5 revealing segregated expression.

BiFC assays

Bimolecular fluorescence complementation assays (BiFC) are similar to "split-GFP" experiments. Here, a yellow fluorescent protein (YFP) VENUS is split into two halves: a N-terminal part VN and a C-terminal part VC. Both parts are non-fluorescent but can complement (when close enough to each other) to generate a fully functional VENUS (see Fig. 6H). Each part is then tagged to one of the test-proteins. When the two test-proteins are close enough (about 7-10 nm apart), fluorescence complementation may occur suggesting physical interactions of the two test-proteins (Fan et al., 2008; Hsu et al., 2011; Shyu et al., 2008).

ACKNOWLEDGEMENTS

We thank the *C. elegans* Core Facility (CECF) Taiwan (funded by the Ministry of Science and Technology, MOST) for providing microinjection setups and worm observation systems. We acknowledge MOST grant MOST 107-2311-B-007-003- to OIW.

REFERENCES

Akhmanova, A., and J.A. Hammer, 3rd. 2010. Linking molecular motors to membrane cargo. *Curr Opin Cell Biol*. 22:479-487.

Alfonso, A., K. Grundahl, J.S. Duerr, H.P. Han, and J.B. Rand. 1993. The Caenorhabditis elegans unc-17 gene: a putative vesicular acetylcholine transporter. *Science*. 261:617-619.

Ali, I., and W.C. Yang. 2020. The functions of kinesin and kinesin-related proteins in eukaryotes. *Cell Adh Migr*. 14:139-152.

Alkema, M.J., M. Hunter-Ensor, N. Ringstad, and H.R. Horvitz. 2005. Tyramine Functions independently of octopamine in the Caenorhabditis elegans nervous system. *Neuron*. 46:247-260.

Avery, L. 1993. The genetics of feeding in Caenorhabditis elegans. *Genetics*. 133:897-917.

Banzato, R., N.M. Pinheiro, C.R. Olivo, F.R. Santana, F. Lopes, L.C. Caperuto, N.O. Câmara, M.A. Martins, I. Tibério, M.A.M. Prado, V.F. Prado, and C.M. Prado. 2021. Long-term endogenous acetylcholine deficiency potentiates pulmonary inflammation in a murine model of elastase-induced emphysema. *Scientific reports*. 11:15918.

Barmaver, S.N., M. Muthaiyan Shanmugam, Y. Chang, O. Bayansan, P. Bhan, G.H. Wu, and O.I. Wagner. 2022. Loss of intermediate filament IFB-1 reduces mobility, density, and physiological function of mitochondria in Caenorhabditis elegans sensory neurons. *Traffic*. 23:270-286.

Bhan, P., M. Muthaiyan Shanmugam, D. Wang, O. Bayansan, C.W. Chen, and O.I. Wagner. 2020. Characterization of TAG-63 and its role on axonal transport in C. elegans. *Traffic*. 21:231-249.

Bhuwania, R., A. Castro-Castro, and S. Linder. 2014. Microtubule acetylation regulates dynamics of KIF1C-powered vesicles and contact of microtubule plus ends with podosomes. *Eur J Cell Biol*. 93:424-437.

Binotti, B., R. Jahn, and J.J. Chua. 2016. Functions of Rab Proteins at Presynaptic Sites. *Cells*. 5.

Brady, S.T., and G.A. Morfini. 2017. Regulation of motor proteins, axonal transport deficits and adult-onset neurodegenerative diseases. *Neurobiol Dis*. 105:273-282.

Brenner, S. 1974. The genetics of Caenorhabditis elegans. *Genetics*. 77:71-94.

Chen, C.W., Y.F. Peng, Y.C. Yen, P. Bhan, M. Muthaiyan Shanmugam, D.R. Klopfenstein, and O.I. Wagner. 2019. Insights on UNC-104-dynein/dynactin interactions and their implications on axonal transport in Caenorhabditis elegans. *J Neurosci Res*. 97:185-201.

Chiba, K., T. Kita, Y. Anazawa, and S. Niwa. 2023. Insight into the regulation of axonal transport from the study of KIF1A-associated neurological disorder. *J Cell Sci*. 136.

Cueva, J.G., J. Hsin, K.C. Huang, and M.B. Goodman. 2012. Posttranslational acetylation of alpha-tubulin constrains protofilament number in native microtubules. *Curr Biol*. 22:1066-1074.

d'Ydewalle, C., J. Krishnan, D.M. Chiheb, P. Van Damme, J. Irobi, A.P. Kozikowski, P. Vanden Berghe, V. Timmerman, W. Robberecht, and L. Van Den Bosch. 2011. HDAC6 inhibitors reverse axonal loss in a mouse model of mutant HSPB1-induced Charcot-Marie-Tooth disease. *Nature medicine*. 17:968-974.

de Castro, B.M., X. De Jaeger, C. Martins-Silva, R.D. Lima, E. Amaral, C. Menezes, P. Lima, C.M. Neves, R.G. Pires, T.W. Gould, I. Welch, C. Kushmerick, C. Guatimosim, I. Izquierdo, M. Cammarota, R.J. Rylett, M.V. Gomez, M.G. Caron, R.W. Oppenheim, M.A. Prado, and V.F. Prado. 2009. The vesicular acetylcholine transporter is required for neuromuscular development and function. *Mol Cell Biol*. 29:5238-5250.

Dompierre, J.P., J.D. Godin, B.C. Charrin, F.P. Cordelieres, S.J. King, S. Humbert, and F. Saudou. 2007. Histone deacetylase 6 inhibition compensates for the transport deficit in Huntington's disease by increasing tubulin acetylation. *J Neurosci*. 27:3571-3583.

Duerr, J.S. 2006. Immunohistochemistry. *WormBook*:1-61.

Dunn, S., E.E. Morrison, T.B. Liverpool, C. Molina-Paris, R.A. Cross, M.C. Alonso, and M. Peckham. 2008. Differential trafficking of Kif5c on tyrosinated and detyrosinated microtubules in live cells. *J Cell Sci*. 121:1085-1095.

Eshun-Wilson, L., R. Zhang, D. Portran, M.V. Nachury, D.B. Toso, T. Lohr, M. Vendruscolo, M. Bonomi, J.S. Fraser, and E. Nogales. 2019. Effects of alpha-tubulin acetylation on microtubule structure and stability. *Proc Natl Acad Sci U S A*. 116:10366-10371.

Even, A., G. Morelli, L. Broix, C. Scaramuzzino, S. Turchetto, I. Gladwyn-Ng, R. Le Bail, M. Shilian, S. Freeman, M.M. Magiera, A.S. Jijumon, N. Krusy, B. Malgrange, B. Brone, P. Dietrich, I. Dragatsis, C. Janke, F. Saudou, M. Weil, and L. Nguyen. 2019. ATAT1-enriched vesicles promote microtubule acetylation via axonal transport. *Sci Adv*. 5:eaax2705.

Factor, S.A., W.M. McDonald, and F.C. Goldstein. 2017. The role of neurotransmitters in the development of Parkinson's disease-related psychosis. *Eur J Neurol*. 24:1244-1254.

Fan, J.Y., Z.Q. Cui, H.P. Wei, Z.P. Zhang, Y.F. Zhou, Y.P. Wang, and X.E. Zhang. 2008. Split mCherry as a new red bimolecular fluorescence complementation system for visualizing protein-protein interactions in living cells. *Biochem Biophys Res Commun*. 367:47-53.

Fan, R., and K.O. Lai. 2022. Understanding how kinesin motor proteins regulate postsynaptic function in neuron. *FEBS J*. 289:2128-2144.

Ferreira-Vieira, T.H., I.M. Guimaraes, F.R. Silva, and F.M. Ribeiro. 2016. Alzheimer's disease: Targeting the Cholinergic System. *Curr Neuropharmacol*. 14:101-115.

Francis, P.T. 2005. The interplay of neurotransmitters in Alzheimer's disease. *CNS Spectr*. 10:6-9.

Garcia-Alloza, M., F.J. Gil-Bea, M. Diez-Ariza, C.P. Chen, P.T. Francis, B. Lasheras, and M.J. Ramirez. 2005. Cholinergic-serotonergic imbalance contributes to cognitive and behavioral symptoms in Alzheimer's disease. *Neuropsychologia*. 43:442-449.

Genova, M., L. Grycova, V. Puttrich, M.M. Magiera, Z. Lansky, C. Janke, and M. Braun. 2023. Tubulin polyglutamylation differentially regulates microtubule-interacting proteins. *EMBO J*. 42:e112101.

Godena, V.K., N. Brookes-Hocking, A. Moller, G. Shaw, M. Oswald, R.M. Sancho, C.C. Miller, A.J. Whitworth, and K.J. De Vos. 2014. Increasing microtubule acetylation rescues axonal transport and locomotor deficits caused by LRRK2 Roc-COR domain mutations. *Nat Commun*. 5:5245.

Guedes-Dias, P., J.J. Nirschl, N. Abreu, M.K. Tokito, C. Janke, M.M. Magiera, and E.L.F. Holzbaur. 2019. Kinesin-3 Responds to Local Microtubule Dynamics to Target Synaptic Cargo Delivery to the Presynapse. *Curr Biol*. 29:268-282 e268.

Guillaud, L., S.E. El-Agamy, M. Otsuki, and M. Terenzio. 2020. Anterograde Axonal Transport in Neuronal Homeostasis and Disease. *Frontiers in molecular neuroscience*. 13:556175.

Guo, W., K. Stoklund Dittlau, and L. Van Den Bosch. 2020. Axonal transport defects and neurodegeneration: Molecular mechanisms and therapeutic implications. *Semin Cell Dev Biol*. 99:133-150.

Hall, D.H., and E.M. Hedgecock. 1991. Kinesin-related gene unc-104 is required for axonal transport of synaptic vesicles in C. elegans. *Cell*. 65:837-847.

Hancock, W.O. 2014. Bidirectional cargo transport: moving beyond tug of war. *Nat Rev Mol Cell Biol*. 15:615-628.

Hirokawa, N., S. Niwa, and Y. Tanaka. 2010. Molecular motors in neurons: transport mechanisms and roles in brain function, development, and disease. *Neuron*. 68:610-638.

Hoerndli, F.J., D.A. Maxfield, P.J. Brockie, J.E. Mellem, E. Jensen, R. Wang, D.M. Madsen, and A.V. Maricq. 2013. Kinesin-1 regulates synaptic strength by mediating the delivery, removal, and redistribution of AMPA receptors. *Neuron*. 80:1421-1437.

Hsu, C.C., J.D. Moncaleano, and O.I. Wagner. 2011. Sub-cellular distribution of UNC-104(KIF1A) upon binding to adaptors as UNC-16(JIP3), DNC-1(DCTN1/Glued) and SYD-2(Liprin-alpha) in C. elegans neurons. *Neuroscience*. 176:39-52.

Hu, C.D., and T.K. Kerppola. 2003. Simultaneous visualization of multiple protein interactions in living cells using multicolor fluorescence complementation analysis. *Nat Biotechnol*. 21:539-545.

Hummel, J.J.A., and C.C. Hoogenraad. 2021. Specific KIF1A-adaptor interactions control selective cargo recognition. *J Cell Biol*. 220.

Ikegami, K., R.L. Heier, M. Taruishi, H. Takagi, M. Mukai, S. Shimma, S. Taira, K. Hatanaka, N. Morone, I. Yao, P.K. Campbell, S. Yuasa, C. Janke, G.R. Macgregor, and M. Setou. 2007. Loss of alpha-tubulin polyglutamylation in ROSA22 mice is associated with abnormal targeting of KIF1A and modulated synaptic function. *Proc Natl Acad Sci U S A*. 104:3213-3218.

Janke, C., and M.M. Magiera. 2020. The tubulin code and its role in controlling microtubule properties and functions. *Nat Rev Mol Cell Biol*. 21:307-326.

Kamath, R.S., M. Martinez-Campos, P. Zipperlen, A.G. Fraser, and J. Ahringer. 2001. Effectiveness of specific RNA-mediated interference through ingested double-stranded RNA in Caenorhabditis elegans. *Genome Biol*. 2:RESEARCH0002.

Kaul, N., V. Soppina, and K.J. Verhey. 2014. Effects of alpha-tubulin K40 acetylation and detyrosination on kinesin-1 motility in a purified system. *Biophys J*. 106:2636-2643.

Kawaguchi, Y., J.J. Kovacs, A. McLaurin, J.M. Vance, A. Ito, and T.P. Yao. 2003. The deacetylase HDAC6 regulates aggresome formation and cell viability in response to misfolded protein stress. *Cell*. 115:727-738.

Kern, J.V., Y.V. Zhang, S. Kramer, J.E. Brenman, and T.M. Rasse. 2013. The kinesin-3, unc-104 regulates dendrite morphogenesis and synaptic development in Drosophila. *Genetics*. 195:59-72.

Klopfenstein, D.R., and R.D. Vale. 2004. The lipid binding pleckstrin homology domain in UNC-104 kinesin is necessary for synaptic vesicle transport in Caenorhabditis elegans. *Mol Biol Cell*. 15:3729-3739.

Lamond, A., D. Buckley, J. O'Dea, and L. Turner. 2021. Variants of SLC18A3 leading to congenital myasthenic syndrome in two children with varying presentations. *BMJ Case Rep*. 14.

Li, L., and X.J. Yang. 2015. Tubulin acetylation: responsible enzymes, biological functions and human diseases. *Cell Mol Life Sci*. 72:4237-4255.

Li, L.B., H. Lei, R.N. Arey, P. Li, J. Liu, C.T. Murphy, X.Z. Xu, and K. Shen. 2016. The Neuronal Kinesin UNC-104/KIF1A Is a Key Regulator of Synaptic Aging and Insulin Signaling-Regulated Memory. *Curr Biol*. 26:605-615.

Maas, C., D. Belgardt, H.K. Lee, F.F. Heisler, C. Lappe-Siefke, M.M. Magiera, J. van Dijk, T.J. Hausrat, C. Janke, and M. Kneussel. 2009. Synaptic activation modifies microtubules underlying transport of postsynaptic cargo. *Proc Natl Acad Sci U S A*. 106:8731-8736.

Maeder, C.I., A. San-Miguel, E.Y. Wu, H. Lu, and K. Shen. 2014. In vivo neuron-wide analysis of synaptic vesicle precursor trafficking. *Traffic*. 15:273-291.

Mahmood, T., and P.C. Yang. 2012. Western blot: technique, theory, and trouble shooting. *N Am J Med Sci*. 4:429-434.

Mathews, E.A., D. Stroud, G.P. Mullen, G. Gavriilidis, J.S. Duerr, J.B. Rand, and J. Hodgkin. 2021. Allele-specific suppression in Caenorhabditis elegans reveals details of EMS mutagenesis and a possible moonlighting interaction between the vesicular acetylcholine transporter and ERD2 receptors. *Genetics*. 218.

Mazzetti, S., F. Giampietro, A.M. Calogero, H.B. Isilgan, G. Gagliardi, C. Rolando, F. Cantele, M. Ascagni, M. Bramerio, G. Giaccone, I.U. Isaias, G. Pezzoli, and G. Cappelletti. 2024. Linking acetylated alpha-Tubulin redistribution to alpha-Synuclein pathology in brain of Parkinson's disease patients. *NPJ Parkinsons Dis*. 10:2.

McIntire, S.L., E. Jorgensen, J. Kaplan, and H.R. Horvitz. 1993. The GABAergic nervous system of Caenorhabditis elegans. *Nature*. 364:337-341.

Mello, C.C., J.M. Kramer, D. Stinchcomb, and V. Ambros. 1991. Efficient gene transfer in C.elegans: extrachromosomal maintenance and integration of transforming sequences. *EMBO J*. 10:3959-3970.

Millecamps, S., and J.P. Julien. 2013. Axonal transport deficits and neurodegenerative diseases. *Nat Rev Neurosci*. 14:161-176.

Mondal, S., S. Ahlawat, K. Rau, V. Venkataraman, and S.P. Koushika. 2011. Imaging in vivo neuronal transport in genetic model organisms using microfluidic devices. *Traffic*. 12:372-385.

Muniesh, M.S., S.N. Barmaver, H.Y. Huang, O. Bayansan, and O.I. Wagner. 2020. PTP-3 phosphatase promotes intramolecular folding of SYD-2 to inactivate kinesin-3 UNC-104 in neurons. *Mol Biol Cell*. 31:2932-2947.

Nass, R., D.H. Hall, D.M. Miller, 3rd, and R.D. Blakely. 2002. Neurotoxin-induced degeneration of dopamine neurons in Caenorhabditis elegans. *Proc Natl Acad Sci U S A*. 99:3264-3269.

Niwa, S., D.M. Lipton, M. Morikawa, C. Zhao, N. Hirokawa, H. Lu, and K. Shen. 2016. Autoinhibition of a Neuronal Kinesin UNC-104/KIF1A Regulates the Size and Density of Synapses. *Cell Rep*. 16:2129-2141.

O'Hagan, R., A. Avrutis, and E. Ramicevic. 2022. Functions of the tubulin code in the C. elegans nervous system. *Mol Cell Neurosci*. 123:103790.

Peris, L., M. Wagenbach, L. Lafanechere, J. Brocard, A.T. Moore, F. Kozielski, D. Job, L. Wordeman, and A. Andrieux. 2009. Motor-dependent microtubule disassembly driven by tubulin tyrosination. *J Cell Biol*. 185:1159-1166.

Reed, N.A., D. Cai, T.L. Blasius, G.T. Jih, E. Meyhofer, J. Gaertig, and K.J. Verhey. 2006. Microtubule acetylation promotes kinesin-1 binding and transport. *Curr Biol*. 16:2166-2172.

Sandoval, G.M., J.S. Duerr, J. Hodgkin, J.B. Rand, and G. Ruvkun. 2006. A genetic interaction between the vesicular acetylcholine transporter VAChT/UNC-17 and synaptobrevin/SNB-1 in C. elegans. *Nat Neurosci*. 9:599-601.

Shyu, Y.J., S.M. Hiatt, H.M. Duren, R.E. Ellis, T.K. Kerppola, and C.D. Hu. 2008. Visualization of protein interactions in living Caenorhabditis elegans using bimolecular fluorescence complementation analysis. *Nat Protoc*. 3:588-596.

Smith, R., H. Chung, S. Rundquist, M.L. Maat-Schieman, L. Colgan, E. Englund, Y.J. Liu, R.A. Roos, R.L. Faull, P. Brundin, and J.Y. Li. 2006. Cholinergic neuronal defect without cell loss in Huntington's disease. *Hum Mol Genet*. 15:3119-3131.

Solinger, J.A., R. Paolinelli, H. Kloss, F.B. Scorza, S. Marchesi, U. Sauder, D. Mitsushima, F. Capuani, S.R. Sturzenbaum, and G. Cassata. 2010. The Caenorhabditis elegans Elongator complex regulates neuronal alpha-tubulin acetylation. *PLoS Genet*. 6:e1000820.

Surana, S., D. Villarroel-Campos, O.M. Lazo, E. Moretto, A.P. Tosolini, E.R. Rhymes, S. Richter, J.N. Sleigh, and G. Schiavo. 2020. The evolution of the axonal transport toolkit. *Traffic*. 21:13-33.

Suzuki, M., T.J. Desmond, R.L. Albin, and K.A. Frey. 2001. Vesicular neurotransmitter transporters in Huntington's disease: initial observations and comparison with traditional synaptic markers. *Synapse*. 41:329-336.

Sze, J.Y., M. Victor, C. Loer, Y. Shi, and G. Ruvkun. 2000. Food and metabolic signalling defects in a Caenorhabditis elegans serotonin-synthesis mutant. *Nature*. 403:560-564.

Teoh, J.S., A. Vasudevan, W. Wang, S. Dhananjay, G. Chandhok, R. Pocock, S.P. Koushika, and B. Neumann. 2022. Synaptic branch stability is mediated by non-enzymatic functions of MEC-17/alphaTAT1 and ATAT-2. *Sci Rep*. 12:14003.

Tien, N.W., G.H. Wu, C.C. Hsu, C.Y. Chang, and O.I. Wagner. 2011. Tau/PTL-1 associates with kinesin-3 KIF1A/UNC-104 and affects the motor's motility characteristics in C. elegans neurons. *Neurobiol Dis*. 43:495-506.

Wagner, O.I., A. Esposito, B. Kohler, C.W. Chen, C.P. Shen, G.H. Wu, E. Butkevich, S. Mandalapu, D. Wenzel, F.S. Wouters, and D.R. Klopfenstein. 2009. Synaptic scaffolding protein SYD-2 clusters and activates kinesin-3 UNC-104 in C. elegans. *Proc Natl Acad Sci U S A*. 106:19605-19610.

Walter, W.J., V. Beránek, E. Fischermeier, and S. Diez. 2012. Tubulin acetylation alone does not affect kinesin-1 velocity and run length in vitro. *PloS one*. 7:e42218.

Wloga, D., E. Joachimiak, and H. Fabczak. 2017. Tubulin Post-Translational Modifications and Microtubule Dynamics. *Int J Mol Sci*. 18.

Wu, G.H., M. Muthaiyan Shanmugam, P. Bhan, Y.H. Huang, and O.I. Wagner. 2016. Identification and Characterization of LIN-2(CASK) as a Regulator of Kinesin-3 UNC-104(KIF1A) Motility and Clustering in Neurons. *Traffic*. 17:891-907.

Xu, F., H. Takahashi, Y. Tanaka, S. Ichinose, S. Niwa, M.P. Wicklund, and N. Hirokawa. 2018. KIF1Bbeta mutations detected in hereditary neuropathy impair IGF1R transport and axon growth. *J Cell Biol*. 217:3480-3496.

Yonekawa, Y., A. Harada, Y. Okada, T. Funakoshi, Y. Kanai, Y. Takei, S. Terada, T. Noda, and N. Hirokawa. 1998. Defect in synaptic vesicle precursor transport and neuronal cell death in KIF1A motor protein-deficient mice. *J Cell Biol*. 141:431-441.

Zadrozny, M., P. Drapich, A. Gasiorowska-Bien, W. Niewiadomski, C.R. Harrington, C.M. Wischik, G. Riedel, and G. Niewiadomska. 2024. Neuroprotection of Cholinergic Neurons with a Tau Aggregation Inhibitor and Rivastigmine in an Alzheimer's-like Tauopathy Mouse Model. *Cells*. 13.

Zhang, Y.V., S.B. Hannan, Z.A. Stapper, J.V. Kern, T.R. Jahn, and T.M. Rasse. 2016. The Drosophila KIF1A Homolog unc-104 Is Important for Site-Specific Synapse Maturation. *Front Cell Neurosci*. 10:207.

Zhu, H., J.S. Duerr, H. Varoqui, J.R. McManus, J.B. Rand, and J.D. Erickson. 2001. Analysis of point mutants in the Caenorhabditis elegans vesicular acetylcholine transporter reveals domains involved in substrate translocation. *J Biol Chem*. 276:41580-41587.

FIGURE LEGENDS

Figure 1: **Candidate screen for genes affecting neurotransmission and simultaneously tubulin PTM in *C. elegans*.** (A) Western blot analysis to investigate changes in tubulin acetylation (upper panel) and tyrosination (lower panel) in various *C. elegans* strains carrying mutations reported to cause synaptic transmission defects. (B) Quantification of band signal intensity from (A, upper panel) using ImageJ software. For tyrosination quantification (A, lower panel) refer to Suppl. Fig. S1. Western blots repeated in triplicates. (C) Simplified scheme of the nervous system in *C. elegans*. (D) Whole mount immunostaining using an anti-acetylated tubulin antibody. The panels display representative confocal images of stacked ALM neurons (C). Upper panel: ALM neurons from N2 wild type worms. Lower panel: ALM neurons from worms with mutations in the *unc-17* gene (*e245* allele). (E) Quantification of images shown in (D) using Image J. Total analyzed neurons per strain: 10. One-way ANOVA with Dunnett's test for multiple comparisons utilized in (B) with *p<0.05. Two-tailed, unpaired Student's t-test with ***p<0.001 in (E). Box and whisker plots represent maximum value, upper quartile, median, lower quartile and minimum value. Scale bars: 10 µm.

Figure 2: **Motor and cargo motility analysis in neurons of living *C. elegans* animals depending on an *unc-17* mutation**. (A) Anterograde and retrograde velocities of kinesin-3 UNC-104 (UNC-104::mRFP) and its major cargo RAB-3 (mCherry::RAB-3) in either wild type N2 or *unc-17*(*e245*) mutants. (B) Number of pauses per 10 µm. (C) Anterograde and retrograde event run lengths. (D) Anterograde and retrograde total run lengths (TTRL). Analyzed events: UNC-104(wt) = 1106, UNC-104(*unc-17*) = 938, RAB-3(wt) = 783 and RAB-3(*unc-17*) = 933. (E) (Left) Kymograph and (right) graphical depiction of kymograph analysis with various motility parameters. Two-tailed, unpaired Student's t-test with *p<0.05, **p<0.01, ***p<0.001, ****p<0.0001. Box and whisker plots represent maximum value, upper quartile, median, lower quartile and minimum value. Scale bars: vertical = 30 s, horizontal = 10 µm.

Figure 3: **Changes in accumulation propensities and distribution patterns of motor and cargo in neurons caused by the *unc-17* mutation.** (A) Schematic diagram of a neuron with blue double-sided arrows indicating the distances travelled from the axon hillock to farther distal regions. (B) Fluorescence images of digitally straightened and stacked ALM neurons taken from different worms expressing UNC-104::mRFP in either wild type or *unc-17* mutants. (C) Representative fluorescence images of stacked ALM neurons taken from different worms expressing mCherry::RAB-3 in either wild type or *unc-17* mutants. (D) Quantification of traveled distances of motor and cargo. (E) Quantification of motor and cargo densities (# particles per 100 µm). (F) Quantification of motor and cargo particle sizes. Total analyzed neurons per strain: 20. Two-tailed, unpaired Student's t-test with *p<0.05, **p<0.01, ***p<0.001, ****p<0.0001. Box and whisker plots represent maximum value, upper quartile, median, lower quartile and minimum value. Scale bar: 10 µm.

Figure 4: **Motor motility after overexpressing/knockdown of acetyltransferase or after adding an ACh neurotransmission inhibitor**. (A-F) Quantification of various motility parameters of UNC-104::mRFP in neurons of living *C. elegans* animals. ACh neurotransmission inhibitor levamisole was added at 1mM to NGM agar and acetyltransferase MEC-17 was either overexpressed (OEX) or knocked down (KD). (A) Anterograde and (B) retrograde velocity. (C) Number of pauses per 10 µm. (D) Total anterograde and (E) retrograde run lengths. (F) Quantification of directional changes (motor reversals, Fig. 2E). (G) Western blot exposing the *mec-17* KD and OEX effect on tubulin acetylation. (H) Band density quantification of gel shown in (G). Analyzed events (n): (A+B) wt(N2) = 2270, wt;EV = 2092, wt;Leva = 2047, wt;MEC-17 *OEX* = 2115, *unc-17*(*e245*);mec-17 *KD* = 1389, *unc-17*(*e245*) = 1093. (C+F) wt(N2) = 44, wt;EV = 40, wt;Leva = 48, wt;MEC-17 *OEX* = 50, *unc-17*(*e245*);mec-17 *KD* = 28, *unc-17*(*e245*) = 32. (D+E) wt(N2) = 12, wt;EV = 16, wt;Leva = 20, wt;MEC-17 *OEX* = 20, *unc-17*(*e245*);mec-17 *KD* = 10, *unc-17*(*e245*) = 20. One-way ANOVA with Dunnett's test for multiple comparisons with *p<0.05, **p<0.005, ***p<0.001, ****p<0.0001 in (A-F) and Kruskal-Wallis one-way ANOVA with Dunnett's test for multiple comparisons with *p<0.05 in (H). For two group comparisons, two-tailed, unpaired Student's t-test with *p<0.05, **p<0.01,

***p<0.001, ****p<0.0001 was used in (A-F) and one-tailed, paired Student's t-test with *p<0.05 in (H). Box and whisker plots represent maximum value, upper quartile, median, lower quartile and minimum value.

Figure 5: ***C. elegans* animals double expressing UNC-104::mRFP/UNC-17::GFP and UNC-104::mRFP/MEC-17::GFP**. (A+B) Colocalization between *Punc-104::unc-104::mrfp* and *Punc-17::unc-17::gfp* in (A) the nerve ring and (B) neurons of the sublateral system. (C+D) Colocalization between *Punc-104::unc-104::mrfp* and *Pmec-17::mec-17::gfp* in (C) head neurons and (D) body neurons. (E) Quantification of colocalization using the intensity correlation quotient (ICQ) method. A<->P = anterior/posterior axis. Analyzed worms: 10 per strain. Graphs represent mean ± STD. Two-tailed, unpaired Student's t-test with **p<0.01. Scale bar: 10 µm.

Figure 6: **Bimolecular fluorescence complementation (BiFC) assay reveals physical *in situ* interactions between UNC-104/UNC-17, UNC-104/MEC-17 and UNC-17/MEC-17**. (A+B) Representative confocal fluorescence images of a worm expressing UNC-104::VN/UNC-17::VC in (A) the head area (nerve ring) and (B) the body area (with ALM highlighted). (C) Empty::VC/UNC-17::VN serving as negative control. (D+E) Worm expressing UNC-104::VN/MEC-17::VC in (D) head neurons and (E) the ALM neuron. (F+G) UNC-17::VN/MEC-17::VC BiFC signals in (F) head neurons and (G) body neurons (ALM highlighted). (H) Graphical depiction of BiFC assay. A<->P = anterior/posterior axis. Single headed arrow pointing to ALM soma. Scale bar: 10 µm. Analyzed worms: 10 per strain. Scale bar: 10 µm.

Figure 7: **Model summarizing the findings from this study**. (A) Proper cargo transport requires unaltered microtubule acetylation levels and functional UNC-17 that interacts with both MEC-17 and UNC-104. (B) Reduced expression of UNC-17 (hypomorph *e245* allele) leads to the freeing of MEC-17 from the UNC-104/UNC-17 complex increasing MT acetylation and concomitantly reducing UNC-104 motility.

FIGURES

FIGURE 1

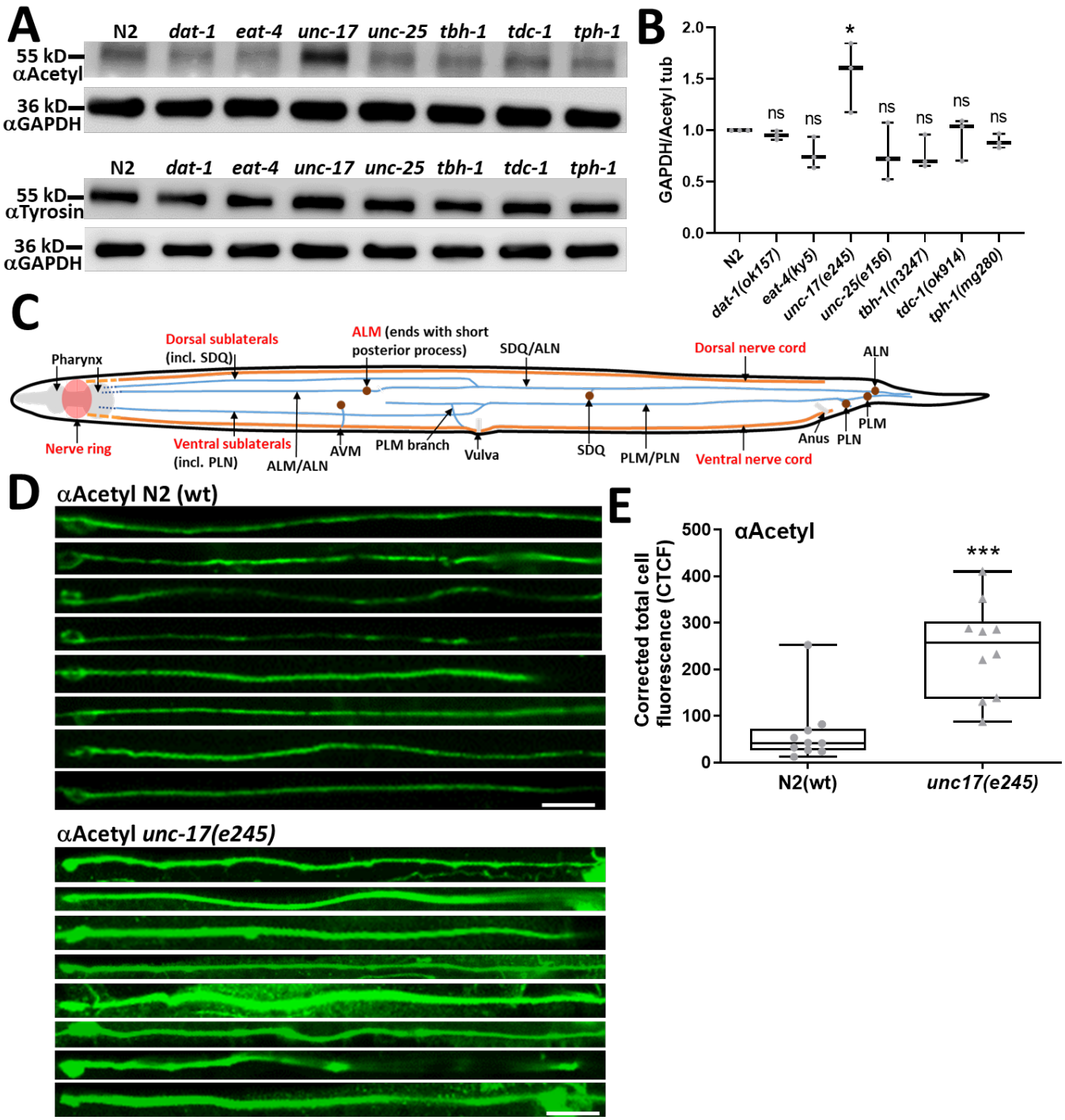

FIGURE 2

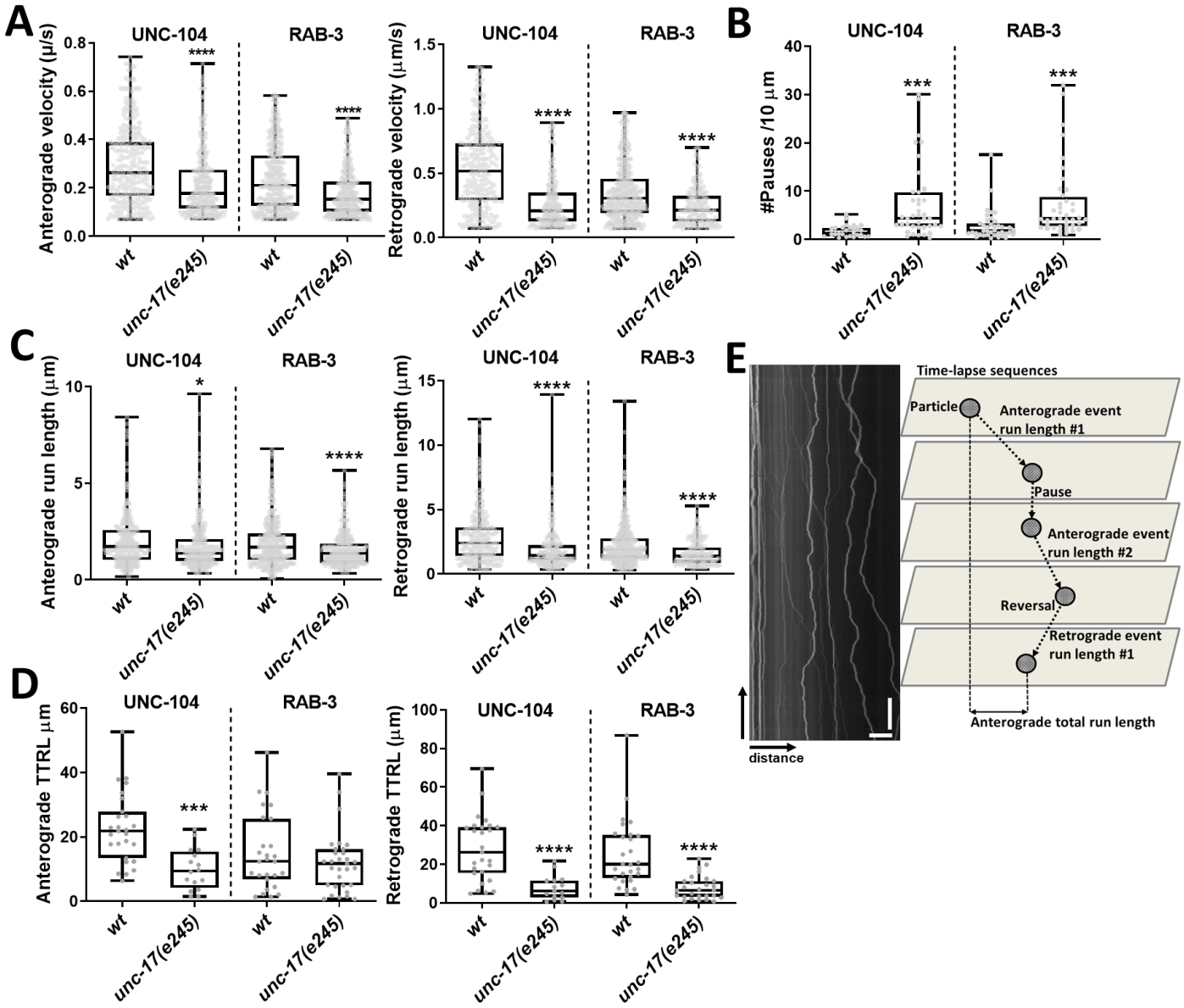
A
Anterograde velocity (μ/s)
UNC-104
RAB-3
****
****
Retrograde velocity (μm/s)
****
****
B
#Pauses /10 μm
***
***
C
Anterograde run length (μm)
*
****
Retrograde run length (μm)
****
****
D
Anterograde TTRL μm
***
Retrograde TTRL (μm)
****
****
wt
unc-17(e245)
E
Time-lapse sequences
Particle
Anterograde event run length #1
Pause
Anterograde event run length #2
Reversal
Retrograde event run length #1
Anterograde total run length
distance

FIGURE 3

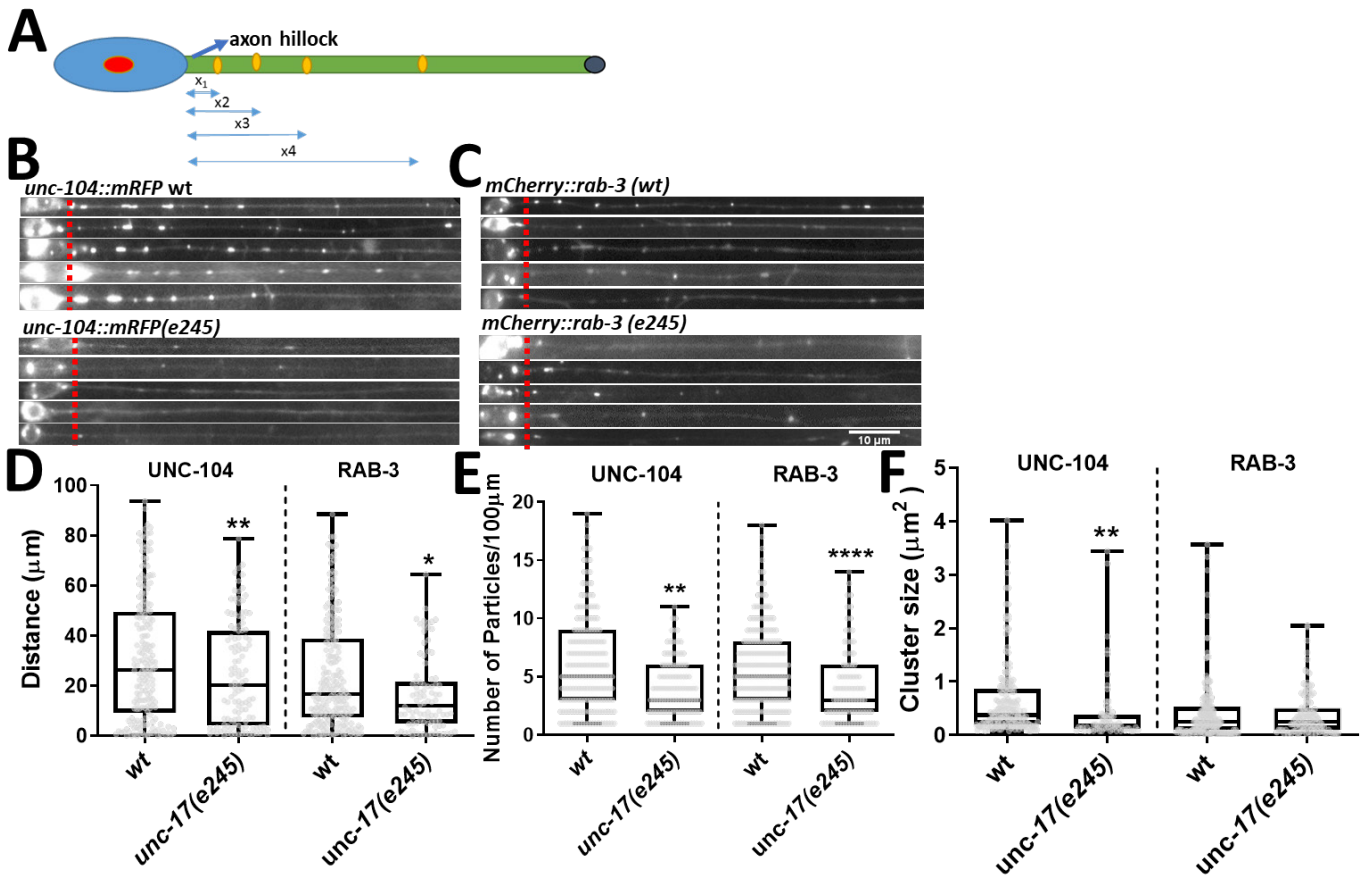
A
axon hillock
x1
x2
x3
x4
B
unc-104::mRFP wt
unc-104::mRFP(e245)
C
mCherry::rab-3 (wt)
mCherry::rab-3 (e245)
10 µm
D
UNC-104
RAB-3
Distance (µm)
100
80
60
40
20
0
**
*
wt
unc-17(e245)
wt
unc-17(e245)
E
UNC-104
RAB-3
Number of Particles/100µm
20
15
10
5
0
**
****
wt
unc-17(e245)
wt
unc-17(e245)
F
UNC-104
RAB-3
Cluster size (µm²)
5
4
3
2
1
0
**
wt
unc-17(e245)
wt
unc-17(e245)

FIGURE 4

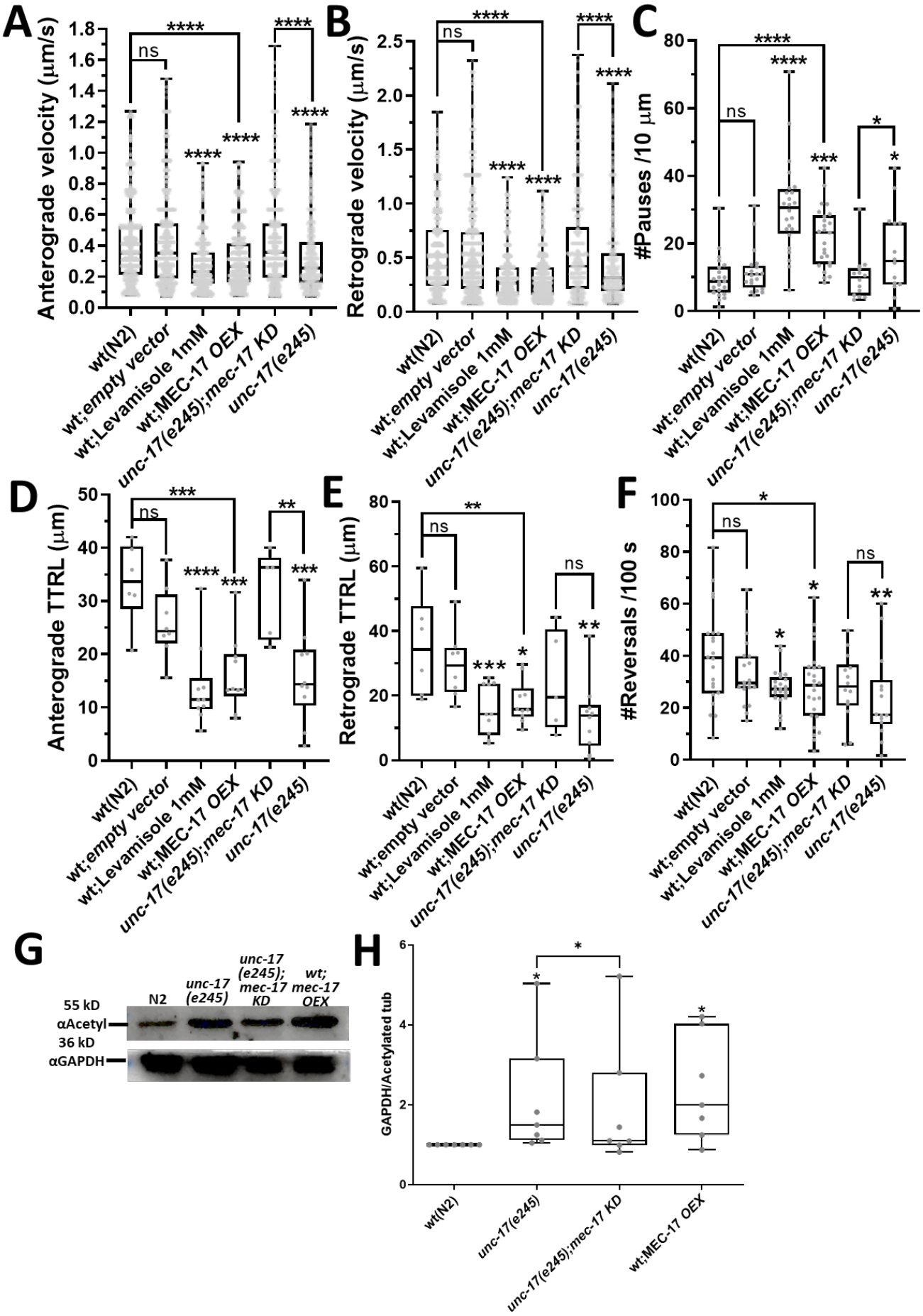
A
Anterograde velocity (μm/s)
B
Retrograde velocity (μm/s)
C
#Pauses /10 μm
D
Anterograde TTRL (μm)
E
Retrograde TTRL (μm)
F
#Reversals /100 s
wt(N2)
wt;empty vector
wt;Levamisole 1mM
wt;MEC-17 OEX
unc-17(e245);mec-17 KD
unc-17(e245)
G
N2
unc-17 (e245)
unc-17 (e245); mec-17 KD
wt; mec-17 OEX
55 kD
αAcetyl
36 kD
αGAPDH
H
GAPDH/Acetylated tub

FIGURE 5

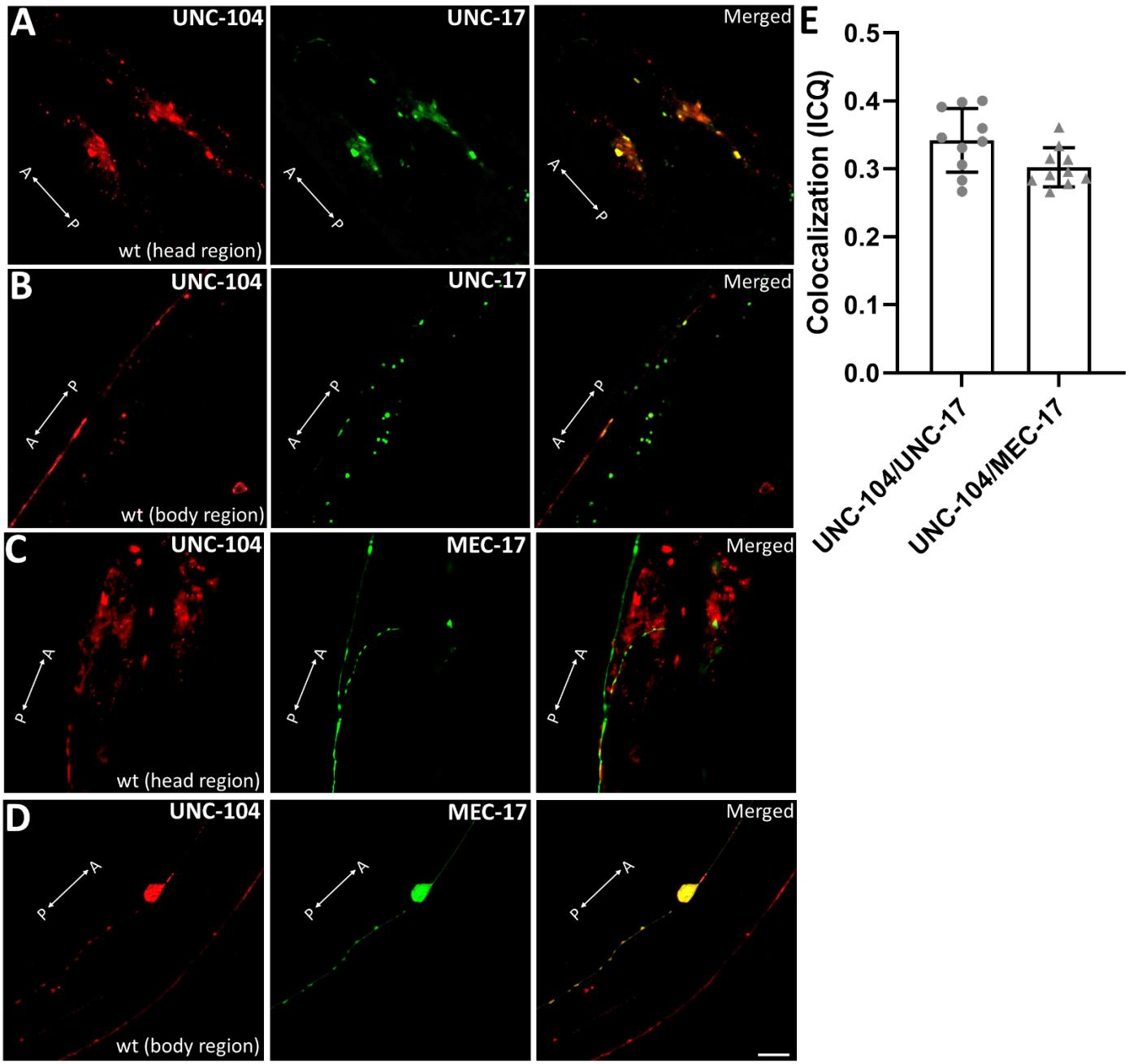
A
UNC-104
UNC-17
Merged
A
P
wt (head region)
B
UNC-104
UNC-17
Merged
wt (body region)
C
UNC-104
MEC-17
Merged
wt (head region)
D
UNC-104
MEC-17
Merged
wt (body region)
E
Colocalization (ICQ)
0.5
0.4
0.3
0.2
0.1
0.0
UNC-104/UNC-17
UNC-104/MEC-17

FIGURE 6

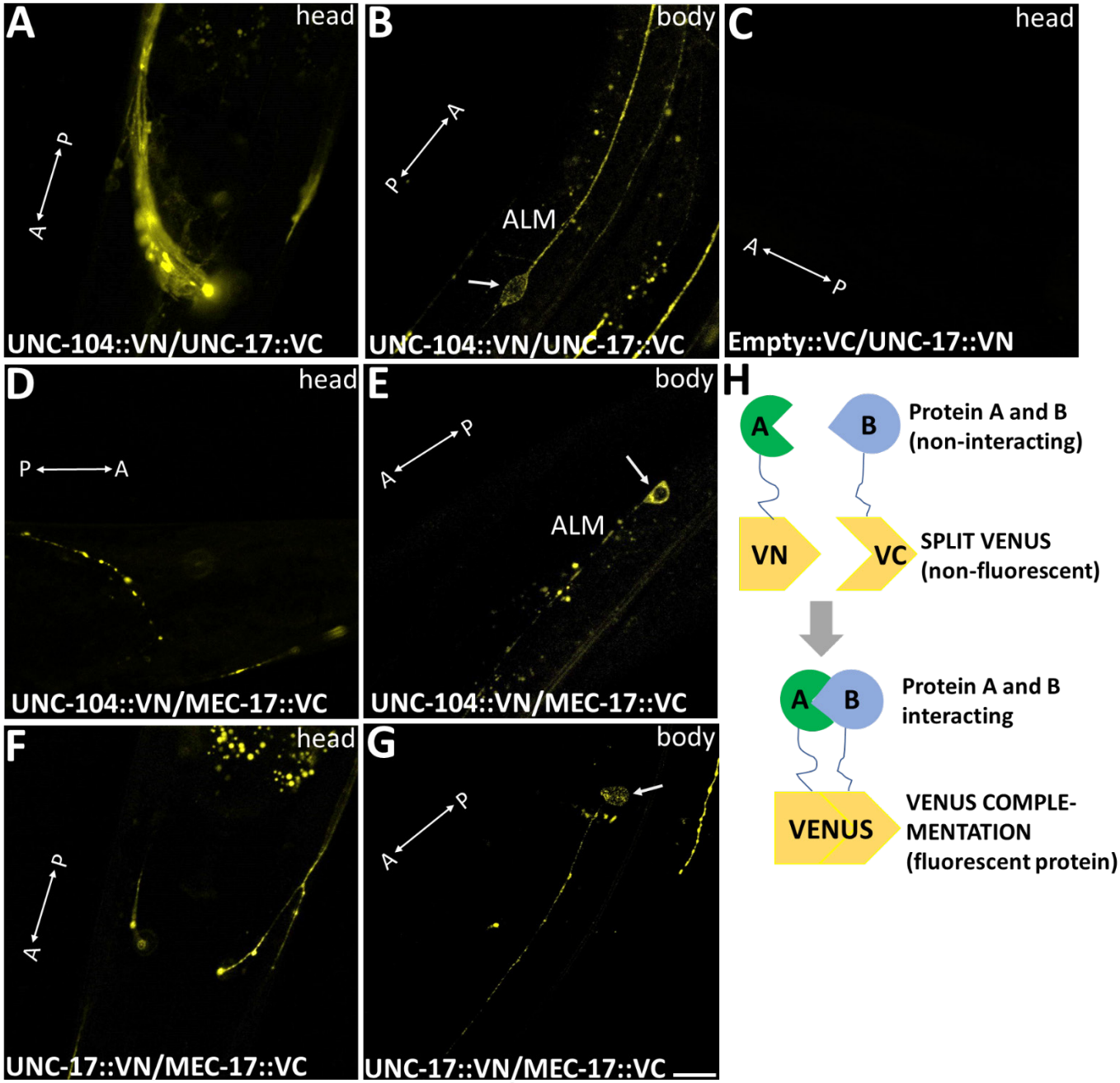
A
head
P
A
UNC-104::VN/UNC-17::VC
B
body
A
P
ALM
UNC-104::VN/UNC-17::VC
C
head
A
P
Empty::VC/UNC-17::VN
D
head
P
A
UNC-104::VN/MEC-17::VC
E
body
P
A
ALM
UNC-104::VN/MEC-17::VC
F
head
P
A
UNC-17::VN/MEC-17::VC
G
body
P
A
UNC-17::VN/MEC-17::VC
H
A
B
Protein A and B
(non-interacting)
VN
VC
SPLIT VENUS
(non-fluorescent)
A
B
Protein A and B
interacting
VENUS
VENUS COMPLE-
MENTATION
(fluorescent protein)

FIGURE 7

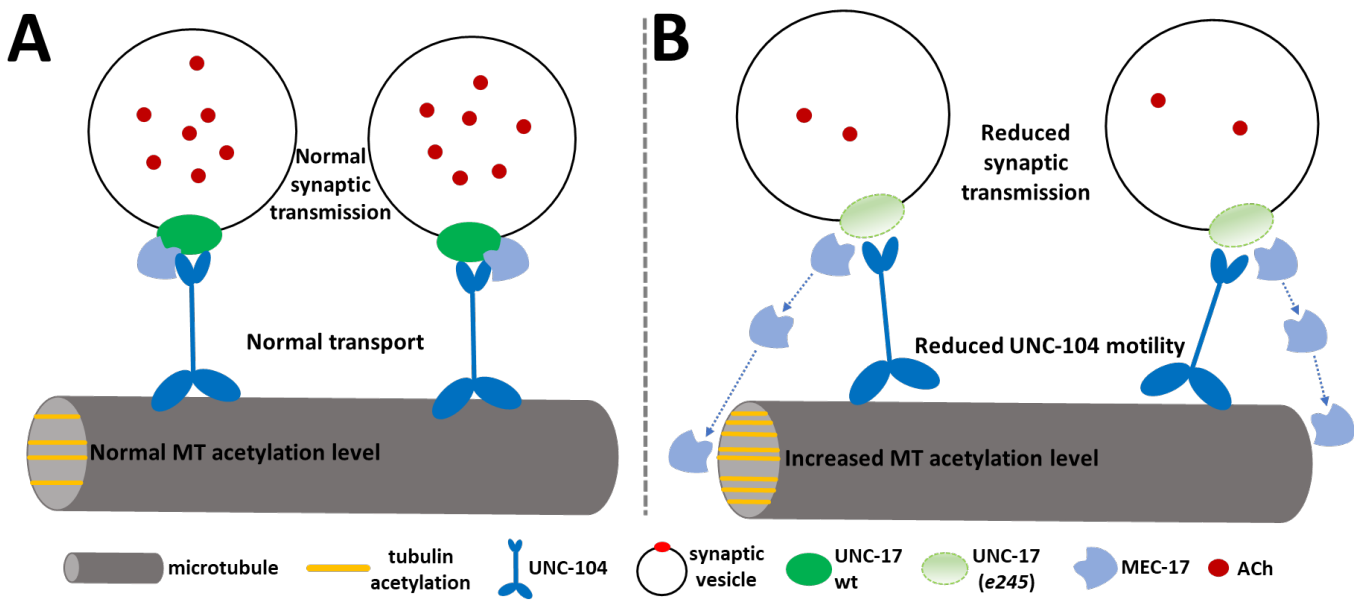
A
Normal synaptic transmission
Normal transport
Normal MT acetylation level
B
Reduced synaptic transmission
Reduced UNC-104 motility
Increased MT acetylation level
microtubule
tubulin acetylation
UNC-104
synaptic vesicle
UNC-17 wt
UNC-17 (e245)
MEC-17
ACh

SUPPLEMENTARY FIGURE LEGENDS

Suppl. Fig. S1: Quantification of band signal intensity from αTyr tubulin gel as shown in Figure 1A, lower panel. One-way ANOVA with Dunnett's test for multiple comparisons utilized with *$p<0.05$. Box and whisker plots represent maximum value, upper quartile, median, lower quartile and minimum value. Scale bars: 10 µm.

Suppl. Fig. S2: Representative kymographs employed to generate data as shown in Fig. 4.

Suppl. Fig. S3: Raw images for cropped gels shown in Figs. 1A and 4G. (A) Upper gel is αAceyl tubulin (55kD) and lower gel is αGAPDH (36kD) as shown Figure 1A (upper panel). (B) Upper gel is αTyrosin tubulin (55kD) and lower gel is αGAPDH (36kD) as shown in Figure 1A (lower panel). (C) Upper gel is αAceyl tubulin (55kD) and lower gel is αGAPDH (36kD) as shown in Figure 4G. Wildcard marks bands specific to the antibody.

SUPPLEMENTARY FIGURES

SUPPL. FIG. S1

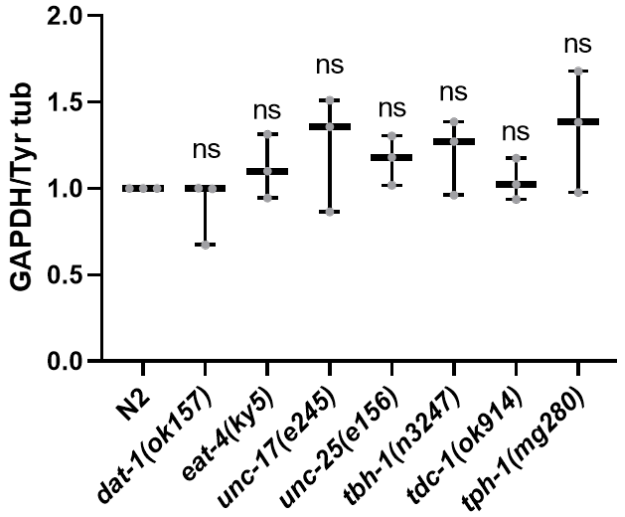

SUPPL. FIG. S2

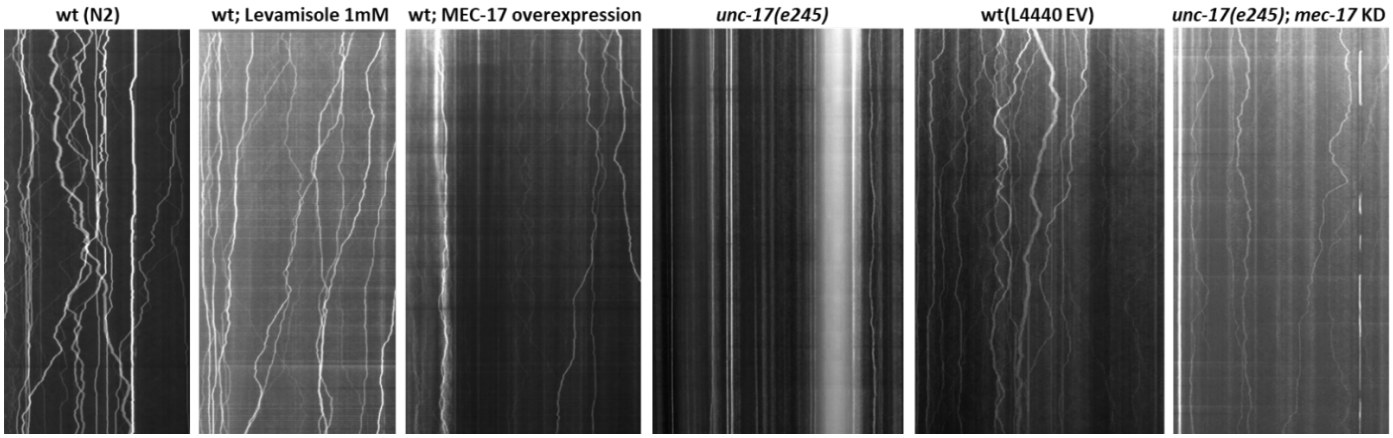

SUPPL. FIG. S3

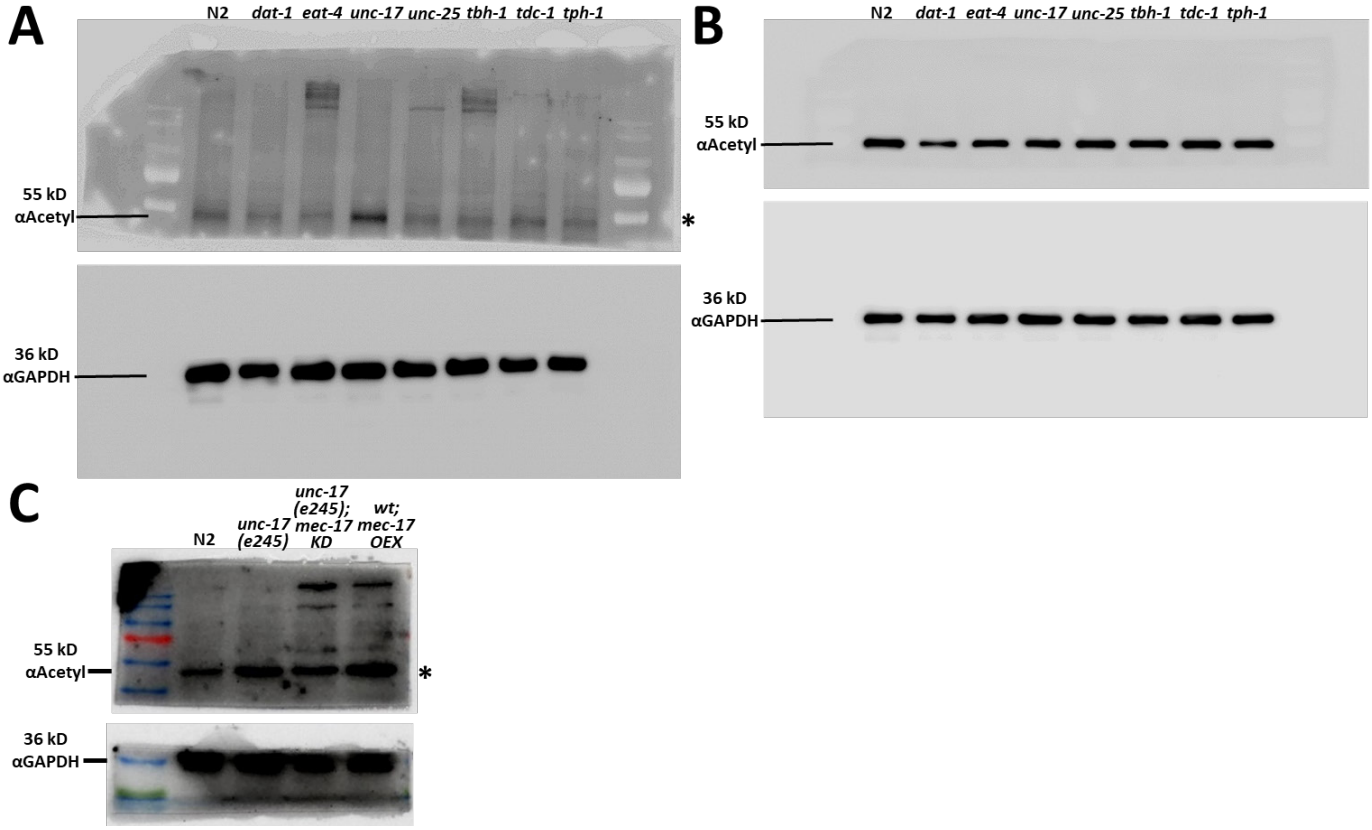
A
N2
dat-1
eat-4
unc-17
unc-25
tbh-1
tdc-1
tph-1
55 kD
αAcetyl
*
36 kD
αGAPDH
B
N2
dat-1
eat-4
unc-17
unc-25
tbh-1
tdc-1
tph-1
55 kD
αAcetyl
36 kD
αGAPDH
C
N2
unc-17 (e245)
unc-17 (e245); mec-17 KD
wt; mec-17 OEX
55 kD
αAcetyl
*
36 kD
αGAPDH